
RePO-VLA: Recovery-Driven Policy Optimization for Vision-Language-Action Model

Weijia Liufu^{1,*} Xiaoyu Guo^{2,3,*†} Ruiyi Chen¹ Jingzhi Liu¹ Kaidong Zhang¹ Xiwen Liang¹
 Jianqi Lin¹ Dawei Sun¹ Yuze Wang⁴ Rongtao Xu⁵ Bingqian Lin¹ Bowen Yang⁶
 Tongtong Cao⁶ Bowen Peng³ Dongyu Zhang¹ Guangrun Wang¹ Min Wang² Liang Lin^{1,3} Xiaodan Liang^{1,3,‡}

¹Sun Yat-sen University ²South China University of Technology ³Peng Cheng Laboratory
⁴Harbin Institute of Technology ⁵Institute of Automation, Chinese Academy of Sciences ⁶Huawei Noah's Ark Lab
 *Equal contribution. †Project leader. ‡Corresponding author.

Abstract

Vision-Language-Action (VLA) models remain brittle in long-horizon, contact-rich manipulation because success-only imitation provides little supervision for execution drift, while failed rollouts are often discarded. We introduce RePO-VLA, a recovery-driven policy optimization framework that assigns distinct roles to success, recovery, and failure trajectories. RePO-VLA first applies Recovery-Aware Initialization (RAI), slicing recovery segments and resetting history so corrective actions depend on the current adverse state rather than the preceding failure. It then learns a Progress-Aware Semantic Value Function (PAS-VF), aligning spatiotemporal trajectory features with instructions and successful references. The resulting labels salvage useful failure prefixes via reliability decay, while low-value labels mark drift and terminal breakdowns, teaching differences among nominal, failed, and corrective actions. The data engine turns adverse states into planner-generated or human-collected corrective rollouts, teaching recovery to the success manifold. Value-Conditioned Refinement (VCR) trains the policy to prefer high-progress actions. At deployment, a fixed high value ($v = 1.0$) biases actions toward the learned success manifold without online failure detectors or heuristic retries. We introduce FRBench, with standardized error injection and recovery-focused evaluation. Across simulated and real-world bimanual tasks, RePO-VLA improves robustness, raising adversarial success from 20% to 75% on average and up to 80% in scaled real-world trials.

1 Introduction

Vision-Language-Action (VLA) models have advanced general-purpose robot control [Kim et al., 2025, Black et al., 2025b], yet a persistent gap remains between nominal benchmark success and reliable long-horizon execution. The gap is especially pronounced in contact-rich bimanual manipulation, where small deviations in grasp pose, object contact, or inter-arm timing can quickly derail a task. These perturbations rarely make the task impossible; instead, they create recoverable adverse states requiring targeted correction before nominal progress can continue. Resilient execution therefore has a temporal structure: useful approach behavior, drift or stalled progress, and correction back to the success manifold.

Current supervision provides little signal for this behavior, despite growing attention to robotic failures [Liu et al., 2023, Ye et al., 2025, Haddadin et al., 2017]. Human-in-the-loop correction [Shi et al., 2024, Wu et al., 2025, Pramanick et al., 2022] and VLM/LLM replanning [Huang et al., 2022, Shinn et al., 2023, Guo et al., 2024] can recover from some high-level mistakes, but they are costly and often disconnected from low-level contact dynamics [Hafner et al., 2023, Ahn et al., 2022]. In practice, most VLA training still relies on supervised fine-tuning (SFT) over successful demonstrations. This creates a failure-utilization blind spot: pure failures are discarded even though their early phases often contain valid approach, contact preparation, or partial-manipulation priors.

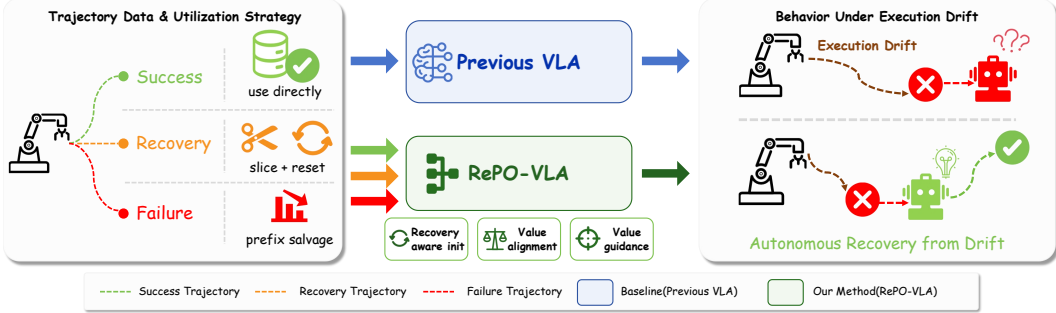


Figure 1: **Recovery-driven trajectory utilization.** Prior VLAs mainly imitate successful demonstrations and often fail under execution drift. RePO-VLA assigns distinct supervision to success, recovery, and failure trajectories, enabling autonomous correction from adverse states.

At the same time, their late phases indicate where behavior drifts away from the success manifold and should be marked as low-value rather than imitated. Recovery demonstrations pose a complementary ambiguity because they contain failed history, adverse states, and corrective actions. Naively imitating the whole sequence conflates the distribution that causes drift with the distribution that repairs it, leading to causal confusion and mode averaging. Sparse binary rewards compound the issue by failing to distinguish useful approach, temporary stagnation, active recovery, and terminal failure.

Figure 1 summarizes the core mismatch: success-only training leaves prior VLAs brittle under drift, while robust recovery requires assigning different roles to success, recovery, and failure trajectories. Failed rollouts should be decomposed rather than discarded, especially as VLA pipelines converge around large-scale imitation and flow-matching backbones. Progress alignment preserves portions close to successful execution; value labels reveal where the same trajectory becomes disadvantageous; and the data engine converts adverse states from injected or policy-induced failures into generated or collected corrective recovery rollouts that teach how to repair them. We propose **RePO-VLA**, a recovery-driven policy optimization framework that learns from successful, failed, and recovered rollouts under a unified progress signal. RePO-VLA first performs **Recovery-Aware Initialization (RAI)**: recovery segments are sliced out and their observation history is reset so corrective skills are conditioned on the current adverse state rather than the preceding mistake. It then learns a **Progress-Aware Semantic Value Function (PAS-VF)** by aligning spatiotemporal video features with language instructions. PAS-VF assigns dense labels to mixed-quality data, isolates error segments from correction segments, and preserves useful early phases of failed trajectories through reliability decay. These labels teach the policy distributional differences among nominal progress, failed drift, and corrective recovery, enabling value-differentiated actions instead of one averaged imitation mode. Finally, **Value-Conditioned Refinement (VCR)** trains the policy to follow high-value behavior. During inference, RePO-VLA fixes the value token to $v = 1.0$, using the learned success manifold as an attractor instead of relying on online failure detectors or hand-coded retry rules.

To evaluate recovery as a first-class capability, we introduce FRBench, a benchmark with standardized error injection, recovery-focused protocols, and simulated and real-world bimanual tasks. FRBench separates nominal execution from recovery execution, making it possible to measure whether a policy can actively repair execution drift rather than merely succeed under clean conditions. Its phase-based protocol conditions recovery on a verified adverse state, preventing improvements in reaching or grasping from being mistaken for true correction. Across FRBench-Sim and real-world adversarial perturbations, RePO-VLA improves recovery success over imitation baselines and shows an empirical recovery-data scaling trend as data density increases.

Our contributions are:

- **RePO-VLA**, a two-phase RAI+VCR framework that eliminates recovery-data causal confusion and structurally reuses failed rollouts: progress alignment preserves useful failure prefixes, low-value labels expose drift-to-correction boundaries, and the data engine converts adverse failure states into generated or collected corrective rollouts for value-conditioned recovery.
- **FRBench**, a recovery benchmark with structured error injection and progress-sensitive evaluation in simulation and real-world bimanual settings.
- **Empirical validation** showing strong recovery gains over SFT baselines and improved recovery with increased recovery-data density.

2 Related Work

2.1 Vision-Language-Action Models

VLA models connect visual-semantic reasoning with robot control. OpenVLA [Kim et al., 2025] casts actions as language tokens, while recent π -series models [Black et al., 2025b,a] use continuous generative policies for dexterous trajectories. RDT-1B [Liu et al., 2025] scales diffusion modeling for bimanual manipulation, and recent efficient or open-source VLA systems such as A1 [Zhang et al., 2026] further improve deployable policy interfaces. Long-horizon extensions add multimodal reasoning [Wen et al., 2025a], memory [Shi et al., 2026], unified diffusion/autoregressive training [Wen et al., 2025b], text-aware visual extraction [Huang et al., 2025], or RL fine-tuning [Guo et al., 2025, Chen et al., 2025a, Physical Intelligence et al., 2025, Zhu et al., 2026]. These works strengthen nominal policy capacity, but most pipelines remain success-demonstration centric and do not specify how failed rollouts should be decomposed into useful prefixes, low-value drift, and corrective recovery.

2.2 Failure Recovery on Robotic Manipulation

Recovery methods include modular replanning, interactive correction, and learned refinement. VLM-guided systems such as ReplanVLM [Mei et al., 2024], REPLAN [Skreta et al., 2024], RACER [Dai et al., 2025], and RoboFAC [Ye et al., 2025] detect precondition errors [Raman et al., 2024] or generate recovery instructions, while affordance-aware hierarchical systems such as A0 [Xu et al., 2025] use structured manipulation affordances to support general robotic manipulation. Interactive methods such as ThriftyDagger [Hoque et al., 2021] and TRANSIC [Jiang et al., 2025] reduce distribution shift through intervention. These external correction layers are useful, but they often remain separate from the learned low-level policy.

Learning-based recovery internalizes this capability. Failure and vulnerability predictors such as FIPER [Römer et al., 2025] and RoboMD [Sagar et al., 2024] estimate risk, while RLFT methods including RLPD [Ball et al., 2023], GRAPE [Zhang et al., 2024], and ConRFT [Chen et al., 2025c] align policies using outcome feedback. These signals are usually sparse or binary [Nakamoto et al., 2023, Mandlekar et al., 2020]. FailSafe [Lin et al., 2025] synthesizes recovery data but still uses SFT, which does not separate erroneous states from corrective actions. RePO-VLA instead uses dense progress labels to train value-conditioned recovery.

2.3 Learning from Mixed-Quality Robotic Data

Offline-to-online RL and preference-style refinement provide useful tools for reusing non-ideal data. RLPD [Ball et al., 2023] improves online RL with offline demonstrations, ConRFT [Chen et al., 2025c] aligns VLA policies through consistency-based reinforced fine-tuning, ReinboT [Zhang et al., 2025] leverages dense returns for visual-language manipulation, and WMPO [Zhu et al., 2026] optimizes VLA behavior with learned world-model feedback. RePO-VLA targets a more specific failure-recovery structure: it gives different semantic roles to successful segments, failure prefixes, terminal drift, and corrective actions. Rather than treating a recovery episode as uniformly positive, RePO-VLA decomposes it into low-value error regions and high-value correction regions; rather than discarding pure failures, it uses semantic progress to retain early useful motion while suppressing terminal breakdowns. This makes recovery learning compatible with mixed-quality datasets where success, failure, and repair behaviors coexist.

3 RePO-VLA

RePO-VLA uses a two-phase curriculum. Phase I, **Recovery-Aware Initialization (RAI)**, adapts the VLA backbone on expert and recovery data while preventing the policy from memorizing the failure history that preceded a correction. Phase II, **Value-Conditioned Refinement (VCR)**, restores the original rolling histories, learns dense progress labels for success, failure, and recovery rollouts, then trains the policy to select actions conditioned on a desired value. This design lets the same policy handle nominal execution and recovery without switching modules at test time.

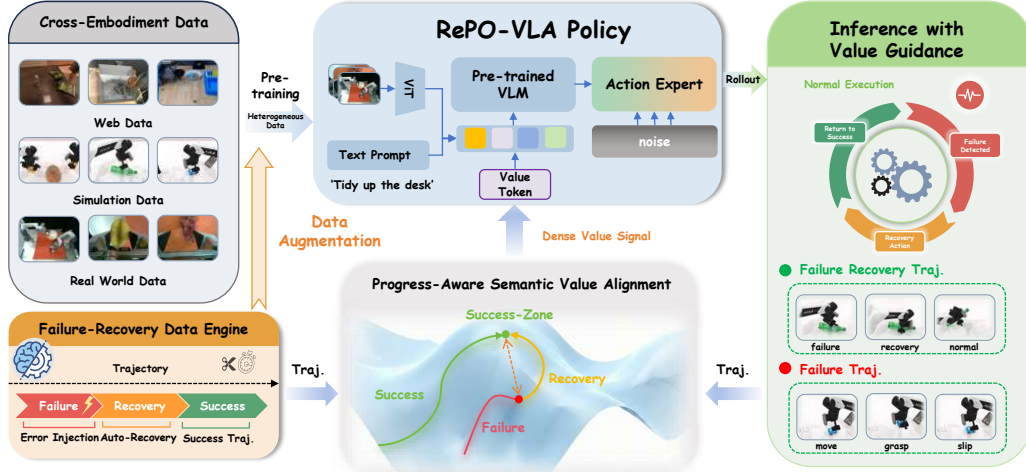


Figure 2: **Overview of RePO-VLA.** The framework builds recovery data, learns a progress-aware semantic value signal, and refines a value-conditioned VLA policy. At inference, constant high-value conditioning ($v = 1.0$) steers execution back toward the success manifold after drift.

3.1 Phase I: Recovery-Aware Initialization (RAI)

RAI initializes the policy with expert demonstrations and recovery actions while avoiding causal confusion [de Haan et al., 2019]. A raw recovery trajectory contains two qualitatively different regions: the failure prefix that leads the system away from progress, and the corrective segment that brings it back. If a transformer policy imitates the full sequence with its observation history intact, it can learn a spurious dependency in which the preceding error is treated as a necessary trigger for recovery. This is undesirable at deployment, where disturbances may appear suddenly and the policy should react to the current adverse observation rather than wait for a familiar failure history.

We address this with Trajectory Slicing with History Reset (TSHR). Given a recovery that starts at t_{rec} , we discard the failure prefix and extract $\tau' = \{(o_t, a_t)\}_{t=t_{rec}}^T$ as an independent correction episode. We then clear the observation-history buffer at the first recovery frame and let it refill normally over the following steps. The resulting reset dataset is denoted $\mathcal{D}_{rec}^{reset}$. These samples expose the policy to adverse states such as an empty gripper, shifted object, or misaligned bimanual pose, but remove the accidental temporal cue that caused them. Thus RAI learns recovery as a state-conditioned skill rather than a replay of a particular failed rollout. Importantly, TSHR is used only for RAI; VCR and deployment use the standard rolling history buffer.

RAI mixes expert data \mathcal{D}_{expert} and reset recovery data $\mathcal{D}_{rec}^{reset}$:

$$\mathcal{L}_{SFT} = -\mathbb{E}_{\tau \sim \mathcal{D}_{expert}} \sum_t \log \pi(a_t | o_t, H_t) - \lambda \mathbb{E}_{\tau' \sim \mathcal{D}_{rec}^{reset}} \sum_t \log \pi(a_t | o_t, H_t^{reset}), \quad (1)$$

where each sum follows the valid horizon of its trajectory, and λ balances nominal imitation and recovery learning.

3.2 Progress-Encoded Semantic Value Learning (PAS-VF)

VCR requires dense labels that preserve useful pre-failure behavior without rewarding terminal breakdowns. A simple zero label for a failed trajectory is too coarse: many failures contain a correct approach, stable pre-contact motion, or partial manipulation before the final deviation. Conversely, assigning a high label to the whole trajectory would reward the terminal error. We therefore learn a self-referential Progress-Aware Semantic Value Function (PAS-VF), denoted $V(\tau)$, that estimates task progress as proximity to successful trajectories in a semantic latent space.

Spatiotemporal Alignment. We map trajectories and language instructions into a shared manifold \mathcal{Z} . This is important because bimanual tasks can be visually redundant: different arm assignments or grasp poses may represent the same semantic progress. A frozen V-JEPA spatiotemporal encoder E_v [Assran et al., 2025] extracts trajectory dynamics, while lightweight adapters produce $z^v = f_\theta(E_v(\tau))$

and $z^l = g_\phi(E_t(l))$. The base encoders remain frozen; only the adapters are optimized, keeping the value model lightweight and focused on progress alignment rather than representation relearning.

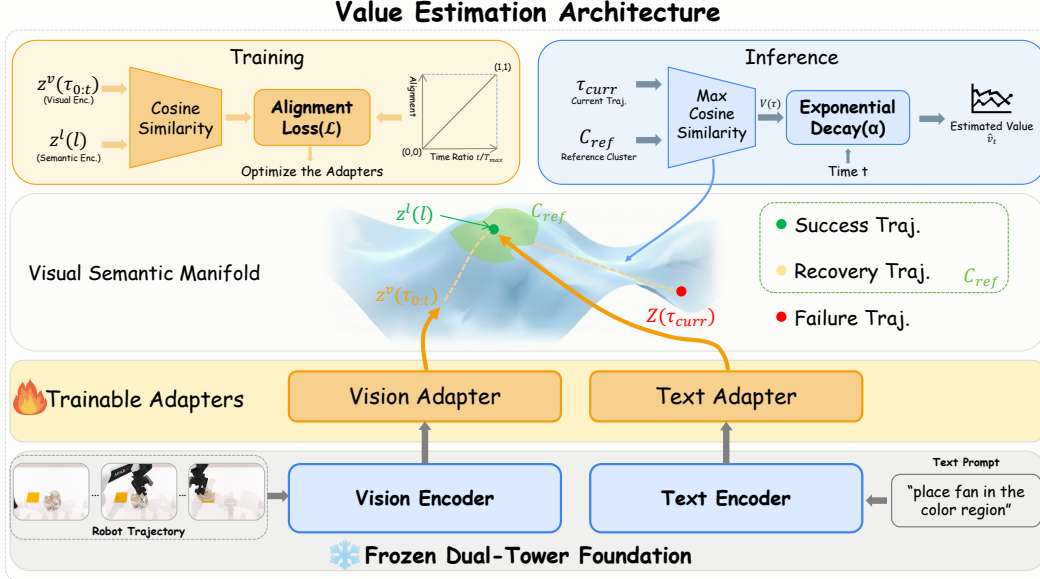


Figure 3: **Semantic value alignment.** Frozen visual and language encoders are projected into \mathcal{Z} ; cosine similarity provides a dense progress signal.

Training: Monotonic Progress Alignment. Adapters are trained on successful trajectories so cosine similarity tracks normalized temporal progress. For each prefix $\tau_{0:t}$, the target progress is t/T_τ , which encourages early prefixes to remain far from the instruction embedding and completed prefixes to align closely with it. With $z_t^v = f_\theta(E_v(\tau_{0:t}))$:

$$\mathcal{L}_{align} = \mathbb{E}_{\tau \in \mathcal{T}_{succ}} \left[\frac{1}{T_\tau} \sum_{t=1}^{T_\tau} \left(\text{CosSim}(z_t^v, z^l) - \frac{t}{T_\tau} \right)^2 \right]. \quad (2)$$

Self-Referential Progress Estimation. After alignment, we use successful executions as an internal reference set. For an unlabeled failure, progress is the nearest similarity to a reference cluster \mathcal{C}_{ref} of successful embeddings:

$$V(\tau_{fail}) = \max_{z \in \mathcal{C}_{ref}} \text{CosSim}(z_{\tau_{fail}}^v, z). \quad (3)$$

Here $z_{\tau_{fail}}^v = f_\theta(E_v(\tau_{fail}))$. This self-referential score avoids manual progress annotation and remains task-relative: a trajectory is valuable when it approaches the successful manifold for its own instruction. Figure 4 visualizes the resulting progress, plateau, and failure regimes.

3.3 Phase II: Value-Conditioned Refinement (VCR)

VCR uses $V(\tau)$ to separate high-value correction from low-value failure behavior across the mixed dataset. Unlike RAI, VCR trains on raw trajectories with intact rolling histories. We denote the original recovery trajectories by \mathcal{D}_{rec}^{raw} and their unmodified history buffer by H_t^{raw} ; for recovery timesteps, H_t^{raw} may contain the preceding failure prefix. This restores the history distribution seen at deployment while using value labels to disambiguate whether recent history corresponds to low-value drift or high-value correction. At deployment, no reset is performed: the policy uses the normal rolling buffer H_t^{oll} and the fixed condition $v = 1.0$, matching the raw-history setting used in VCR.

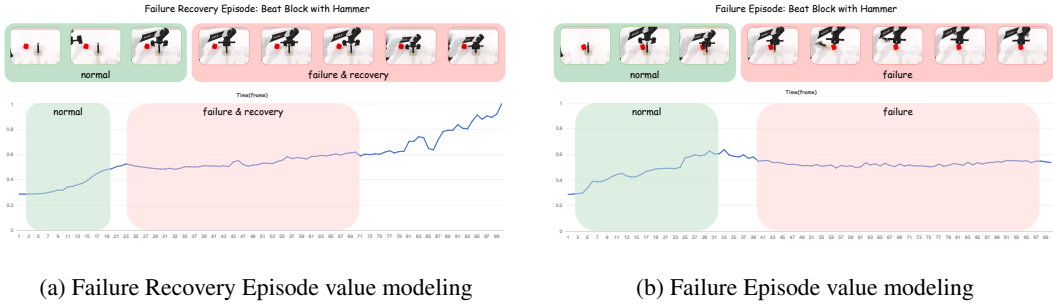


Figure 4: Visualization of the Progress-Aware Value Landscape.

3.3.1 Progress-Aware Hindsight Labeling

We construct a continuous value landscape over the raw mixed dataset by assigning each frame a dense label $v_t \in [0, 1]$. The labels are designed to separate behavior quality rather than trajectory identity:

- **Success and recovery:** successful trajectories τ_{succ} and effective recovery suffixes $\tau_{rec}^+ \subset \mathcal{D}_{rec}^{raw}$ receive $v_t = 1.0$, since these frames contain actions that either maintain or restore progress.
- **Error segments:** deviating recovery prefixes $\tau_{rec}^- \subset \mathcal{D}_{rec}^{raw}$ receive $v_t = 0.0$. This explicitly tells the policy that the actions leading into the adverse state should not be averaged with the corrective actions that follow, even though both are observed under the same raw rolling history.
- **Pure failures:** failed rollouts τ_{fail} keep early kinematic priors through reliability decay,

$$v_t = V(\tau_{fail}) \cdot \left(1 - \frac{t}{T}\right)^\alpha, \quad \forall t \in \tau_{fail}, \quad (4)$$

with $\alpha = 3.0$. This retains useful early motion while rapidly down-weighting states near irreversible failure, reflecting the physical intuition that action utility degrades quickly as irreversible failure approaches.

3.3.2 Goal-Conditioned Architecture and Inference

Value-Conditioned Training. We augment the flow-matching $\pi_{0.5}$ policy [Black et al., 2025a] with a value token $e_{val} = \text{MLP}_{val}(v_t)$. The transformer attends to this token together with visual, language, and history tokens, allowing the same adverse observation and history to map to different action modes depending on desired progress. We fine-tune on $\mathcal{D}_{total} = \mathcal{D}_{succ} \cup \mathcal{D}_{rec}^{raw} \cup \mathcal{D}_{fail}$:

$$\mathcal{L}_{VCR} = -\mathbb{E}_{\tau \sim \mathcal{D}_{total}} \left[\sum_{t=1}^{T_\tau} \log \pi_\theta(a_t | o_t, H_t, l, e_{val}(v_t)) \right]. \quad (5)$$

Goal-Conditioned Autonomous Recovery. During deployment, we do not estimate $V(\tau)$ online, clear H_t , or run an online failure detector. The policy uses the standard rolling buffer H_t^{roll} and a fixed target value $v = 1.0$ at every step. This matches VCR, where corrective actions are trained with intact failure histories in H_t^{raw} . Thus, when recent low-value observations remain in the buffer, the high-value token selects the corrective branch learned during VCR, enabling recovery without explicit failure triggers or retry rules.

4 FRBench

FRBench evaluates whether bimanual policies can restore task progress after physical breakdowns. Unlike success-only suites, it separates nominal proficiency from corrective capability through controlled adverse-state projection. FRBench spans RoboTwin simulation [Chen et al., 2025b] and real-world tasks, with 23,453 simulated episodes over 46 tasks. Recovery evaluation is conditional on verified adverse states, so improvements in reaching or grasp timing are not mistaken for true correction.

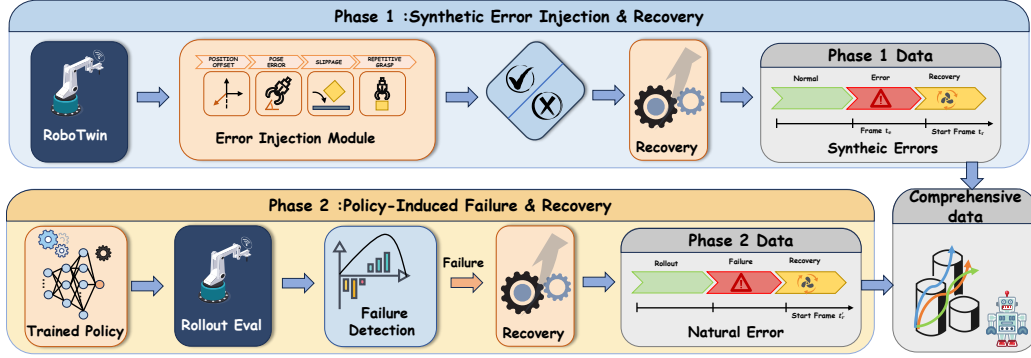


Figure 5: **Failure-Recovery Data Engine.** Recovery data combines control-intercepted error injection with policy-induced rollouts.

Phase-based protocol. FRBench evaluates recovery as a controlled state-transition problem: each trial passes through nominal execution, error projection, and recovery execution, so recovery success is conditioned on a verified adverse state rather than confounded by approach quality.

Table 1: **FRBench phase-based evaluation protocol.** The protocol isolates nominal task competence from corrective behavior after a controlled physical breakdown.

Phase	State	Control or intervention	Isolated measurement
Nominal	$\phi_t = \text{NOMINAL}$	Policy executes under clean or randomized conditions.	Baseline reaching, grasping, and task progress.
Error	$\phi_t = \text{ERROR}$	Structured E1–E4 perturbation projects the scene into an adverse state.	Reproducible physical breakdown independent of policy scoring.
Recovery	$\phi_t = \text{RECOVERY}$	The policy continues from the adverse state without external retry logic.	Corrective actions that restore task progress.

4.1 Failure-Recovery Data Engine

The data engine in Fig. 5 supplies recovery supervision through two complementary sources, balancing broad coverage with policy-specific realism:

Interception-Based Synthetic Injection. We hook expert-planner execution nodes and inject targeted errors (E1–E4) during critical segments such as grasping or lifting. A hierarchical planner then restores the task state. The synthetic stream provides controlled coverage of common physical breakdowns while preserving task-level consistency.

Policy-Induced Rollouts. We also collect closed-loop failures from trained base policies and let the expert planner intervene, yielding in-distribution recovery data for model-specific drift. Synthetic errors alone cannot fully capture the compounding execution drift native to learned visual perception and action generation, so this stream targets the failure neighborhoods that policies actually visit.

Both sources are merged into raw recovery trajectories \mathcal{D}_{rec}^{raw} for VCR; RAI derives $\mathcal{D}_{rec}^{reset}$ from them via TSHR. The synthetic stream provides controlled coverage of common physical breakdowns, while the policy-induced stream captures the errors that actually arise from learned visual perception and action generation.

Interception Sequence. The generation process follows five controlled steps: (1) the expert oracle computes a successful reference trajectory τ_{nom} ; (2) the data engine monitors task progress and intercepts a critical execution node such as grasp or lift; (3) an E1–E4 perturbation overrides the nominal action; (4) the perturbed execution projects the robot into an adverse state; and (5) a hierarchical recovery planner synthesizes corrective actions to restore the task state. This sequence creates paired failure-recovery episodes without changing the base task pipeline.

Perturbation Taxonomy. Let the nominal action at timestep t be $a_t = [p_t, R_t, g_t]$, where $p_t \in \mathbb{R}^3$ is end-effector position, $R_t \in SO(3)$ is orientation, and g_t is gripper state. FRBench uses four deterministic overrides:

- **E1:** `premature_close`. The gripper closes early during approach, often causing an empty grasp or partial contact: $g'_t = g_{closed}$ for $t \in [t_{approach}, t_{approach} + N_{hold}]$.

- **E2: grasp_slip.** The gripper opens during lift for a deterministic window, abruptly breaking contact forces: $g'_t = g_{open}$ for $t \in [t_{lift}, t_{lift} + 30]$.
- **E3: grasp_position_offset.** A cm-level translational offset perturbs the target pose: $p'_t = p_t + \delta p_{trans}$, where $\delta p_{trans} \sim \mathcal{U}(-d, d)$.
- **E4: grasp_orientation_mismatch.** A large rotational mismatch with lateral stabilization induces realistic misgrasp: $R'_t = R_t \cdot \Delta R_{err}$ with $p'_t = p_t + \delta p_{lat}$.

The same taxonomy is applied across FRBench-Sim and FRBench-Real via platform-specific implementations.

Detection and Real-World Recovery. In simulation, failure events are triggered when execution exceeds the maximum nominal success duration,

$$\mathcal{F}_t = \mathbb{I}(t > T_{\max}), \quad T_{\max} = \max_{i \in \{1, \dots, n\}} (T_{succ}^i). \quad (6)$$

This captures progress stagnation and loops that may not cause immediate collision or object-drop events. In the real world, recovery episodes are curated via human teleoperation: operators intentionally initialize adverse states, such as partial object slippage or inter-arm misalignment, and demonstrate corrective trajectories back to the success manifold.

Table 2: **FRBench-Sim dataset statistics.** Counts summarize the generated trajectory corpus and aggregate error-injection coverage.

Category	Count	Description
Total episodes	23,453	All generated bimanual manipulation episodes
Nominal success	17,061	Successful trajectories without injected failures
Failure-recovery	6,392	Verified multi-step recovery trajectories
Task diversity	46	Distinct bimanual tasks across daily and industrial settings
Environment modes	2	Clean and randomized task instantiations
E1: Premature Close	8,022	Early gripper closure during approach
E2: Grasp Slip	3,516	Forced gripper opening during lift
E3: Position Offset	4,686	Translational grasp target offset
E4: Orientation Mismatch	688	Rotational mismatch with lateral stabilization

Note. Error-type counts exceed the 6,392 filtered recovery trajectories due to combinatorial testing across environments before final sequence filtering.

5 Experiment

5.1 Simulation Evaluation (FRBench-Sim)

We evaluate FRBench-Sim on Dynamic Grasp Failure, a proxy for contact anomalies such as `grasp_slip` and `premature_close`. This perturbation is deliberately low-level: it does not change the task instruction, but it breaks object control and requires the policy to re-enter a valid grasping state. Baselines include RDT [Liu et al., 2025], GO-1 [Bu et al., 2025], π_0 [Black et al., 2025b], $\pi_{0.5}$ [Black et al., 2025a], and Phase I ablations.

Protocol. We run 50 rollouts per task in RoboTwin Clean and Random settings. Recovery trials inject a grasp disturbance by holding the gripper open for 30 frames ($\sim 1s$) at grasp initiation, forcing the policy to re-establish object control. The recovery-data visualizations in Section 6.1 show representative injected failures and corrective trajectories.

Table 3 shows two effects. First, Phase I improves nominal robustness: under randomization, its average success remains stable from 44.6 to 44.0, whereas π_0 drops from 33.9 to 12.9. This indicates that recovery-aware initialization does not trade away base task competence. Second, under injected failures, full RePO-VLA improves over $\pi_{0.5}$ from 15.0/15.4 to 37.0/43.0. The gain is largest in tasks where the perturbation forces a genuine re-grasp or re-alignment, supporting the hypothesis that dense value conditioning helps the policy return to the success manifold rather than continuing the nominal plan. Baseline models such as RDT and GO-1 show lower success under randomized conditions, highlighting their limited robustness.

Table 3: **FRBench-Sim success rate (%)**. We report nominal and injected-failure success over ten RoboTwin tasks. Method labels include venue year and citation; \uparrow means higher is better, Δ reports average gain over the corresponding $\pi_{0.5}$ baseline, and gray rows denote RePO-VLA variants.

Model	Split	Task Success Rate (%) \uparrow										Avg. \uparrow	Δ Avg. \uparrow
		Blocks RGB	Blocks Size	Hang Mug	Lift Pot	Move Stap.	Open Laptop	Place Bread	Place Can	Place Mouse	Press Stap.		
Standard (nominal)													
RDT (ICLR'25) [Liu et al., 2025]	Clean	3	0	23	72	2	59	5	19	1	41	22.5	—
	Rand.	0	0	16	9	0	32	1	6	0	24	8.8	—
GO-1 (arXiv'25) [Bu et al., 2025]	Clean	7	2	0	92	3	65	2	29	15	66	28.1	—
	Rand.	3	2	0	92	4	60	1	37	10	51	26.0	—
π_0 (RSS'25) [Black et al., 2025b]	Clean	19	7	11	84	0	85	23	41	7	62	33.9	—
	Rand.	5	1	3	36	2	46	1	5	1	29	12.9	—
$\pi_{0.5}$ (CoRL'25) [Black et al., 2025a]	Clean	30	20	6	28	10	52	26	30	12	60	27.4	—
	Rand.	48	22	10	20	16	74	44	20	28	54	<u>33.6</u>	—
w/o Fail	Clean	82	54	4	38	26	62	34	48	38	0	44.6	(+17.2)
	Rand.	68	56	8	36	18	54	50	46	48	0	44.0	(+10.4)
Injected failure													
$\pi_{0.5}$ (CoRL'25) [Black et al., 2025a]	Clean	20	2	0	6	0	64	0	0	0	58	15.0	—
	Rand.	22	6	0	0	0	68	0	0	4	54	<u>15.4</u>	—
RePO-VLA	Clean	70	60	0	30	0	90	20	10	10	80	37.0	(+22.0)
	Rand.	80	40	20	0	30	100	60	10	20	70	43.0	(+27.6)

Tasks. Blocks RGB/Size: Blocks Ranking RGB/Size; Move Stap.: Move Stapler Pad; Place Bread/Can/Mouse: Place Bread Skillet/Place Can Basket/Place Mouse Pad; Press Stap.: Press Stapler. Bold/underline indicate best/second-best results within each block.

Table 4: **FRBench-Real success rate (%)**. Results are averaged over 10 trials per task under standard and adversarial settings. Method labels include venue year and citation; \uparrow means higher is better, Δ reports improvement over $\pi_{0.5}$ in the same condition, gray columns denote RePO-VLA variants, bold/underline mark best/second-best results, and green/red Δ values denote gains/losses.

Task	Standard (No Perturbation) \uparrow					Adversarial (With Perturbation) \uparrow				
	π_0 (RSS'25) [Black et al., 2025b]	$\pi_{0.5}$ (CoRL'25) [Black et al., 2025a]	Phase I	Full (1x)	Δ	π_0 (RSS'25) [Black et al., 2025b]	$\pi_{0.5}$ (CoRL'25) [Black et al., 2025a]	Phase I	Full (1x)	Δ
Pour Water	40	30	60	50	(+20)	20	20	60	30	(+10)
Cook Vegetable	10	10	30	40	(+30)	0	10	30	30	(+20)
Tidy Desk	20	20	40	40	(+20)	10	30	40	30	(+10)
Fold Towel	40	40	40	30	(-10)	20	20	20	30	(+10)
Avg.	27.5	25.0	42.5	<u>40.0</u>	(+15.0)	12.5	20.0	37.5	<u>30.0</u>	(+10.0)

5.2 Real-World Evaluation & Recovery Data Scaling

We evaluate on two Dobot X-Trainer arms across *Vegetable Preparation*, *Towel Folding*, *Desk Organization*, and *Liquid Pouring*. These tasks cover precision pouring, deformable-object manipulation, workspace rearrangement, and bimanual coordination. Each task uses 200 expert demonstrations and 50 teleoperated recovery episodes. In the adversarial setting, a human injects dynamic displacement, kinematic interference, or forced slippage at critical phases, producing disturbances that are difficult to script exactly but common in physical deployments. We compare against π_0 and $\pi_{0.5}$ [Black et al., 2025b,a]. Qualitative task settings are shown in Section 6.2.

Baseline Fragility and Data Scaling. Table 4 shows that imitation baselines degrade under adversarial perturbations, confirming that nominal imitation alone does not provide reliable corrective behavior. Phase I raises adversarial average success to 37.5%, demonstrating the value of explicitly exposing the policy to recovery actions. Full (1x) improves over $\pi_{0.5}$ but does not yet dominate Phase I, revealing a data-density bottleneck: value-conditioned refinement must model a more diverse distribution of natural errors than Phase I imitation, and sparse recovery data can make that value landscape noisy.

Table 5 and Fig. 6 report the corresponding recovery-data scaling study. Doubling and quadrupling recovery data reduces this bottleneck: Full** (4x) improves average standard and adversarial success over $\pi_{0.5}$ by 45 and 55 points, respectively, and surpasses Phase I under adversarial perturbations.

Table 5: **Recovery-data scaling study (%)**. We increase real-world recovery data from 1x to 2x and 4x on two representative tasks. Method labels include venue year and citation; \uparrow means higher is better, $\Delta_{4x-0.5}$ and Δ_{4x-I} compare Full** (4x) with $\pi_{0.5}$ and Phase I, bold/underline mark best/second-best results, and green/red Δ values denote gains/losses.

Condition	Task	Baselines		RePO-VLA Variants				Improvement \uparrow	
		π_0 (RSS'25) [Black et al., 2025b]	$\pi_{0.5}$ (CoRL'25) [Black et al., 2025a]	Phase I	Full (1x)	Full* (2x)	Full** (4x)	$\Delta_{4x-0.5}$	Δ_{4x-I}
Standard	Pour Water	40	30	60	50	<u>80</u>	90	(+60)	(+30)
	Fold Towel	40	40	40	30	<u>60</u>	70	(+30)	(+30)
	Avg.	40	35	50	40	<u>70</u>	80	(+45)	(+30)
Adversarial	Pour Water	20	20	60	30	70	80	(+60)	(+20)
	Fold Towel	20	20	20	30	<u>60</u>	70	(+50)	(+50)
	Avg.	20	20	40	30	<u>65</u>	75	(+55)	(+35)

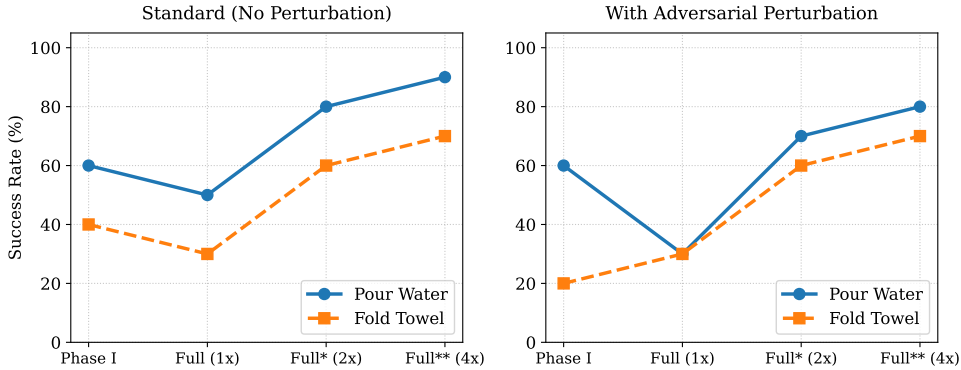


Figure 6: **Recovery-data scaling trends**. Success rates on Pour Water and Fold Towel improve as real-world recovery data increases from 1x to 4x under both standard and adversarial settings, matching the scaling study in Table 5.

This empirical trend suggests that RePO-VLA benefits not merely from a few recovery examples, but from denser coverage of the state-action neighborhoods around realistic failures.

5.3 Ablation Studies

We ablate history reset, value guidance, and decay rate α .

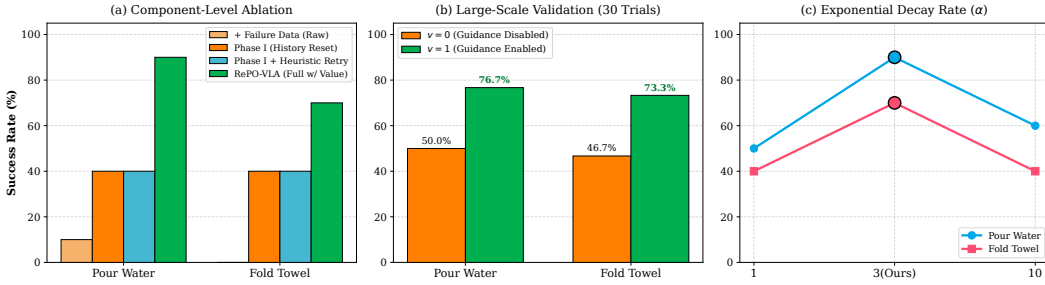


Figure 7: **Real-world ablations**. (a) Component ablations isolate history reset and value guidance under matched recovery data. (b) A 30-trial validation shows that enabling $v = 1$ consistently improves success. (c) The decay sweep identifies $\alpha = 3$ as the best balance between preserving useful failure prefixes and penalizing terminal breakdowns.

Component and Value Guidance. Figure 7(a) shows that raw failure-recovery data without history reset causes causal confusion, while TSHR restores recovery. The heuristic retry baseline remains weaker than value guidance even when trained with the same recovery data, indicating that the key benefit is not merely attempting the task again, but conditioning the action distribution toward high-progress regions. In the 30-trial validation of Fig. 7(b), enabling $v = 1$ consistently improves

both tasks, suggesting that value conditioning provides a stable deployment-time control signal rather than a fragile one-off prompt.

Decay Rate. Figure 7(c) identifies $\alpha = 3$ as the best trade-off: $\alpha = 1$ under-penalizes near-terminal failures, while $\alpha = 10$ discards useful early approach behavior. This supports the intended role of reliability decay: pure failures should not be treated as demonstrations of success, but neither should their early, physically meaningful motions be wasted.

6 Qualitative Visualization

6.1 Visualization of Recovery Data

We visualize representative recovery samples generated by the automated pipeline in RoboTwin with the ALOHA-Agilex embodiment. The examples illustrate the full recovery workflow, from physics-driven error injection to autonomous corrective execution.

For each of the four core error types (E1–E4), we provide six task examples across both Clean and Random (domain-randomized) environments to ensure visual and kinematic diversity. Each task sequence consists of 9 keyframes sampled from a single episode:

- Frames 1-3 (Error): the “Error Attempt” phase, where physics-driven perturbations rather than simple Gaussian noise induce a natural failure.
- Frames 4-8 (Recovery): the “Recovery” phase, with planner-based trajectories that include re-perception and corrective actions.
- Frame 9 (Normal): the resumed “Normal” execution phase from the corrected state.

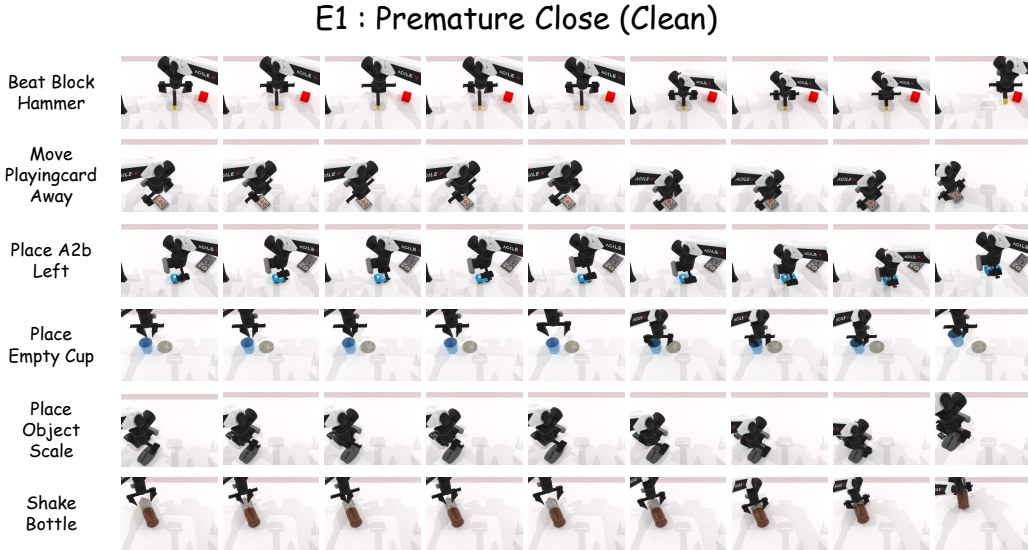


Figure 8: Premature Close (Clean)

6.2 Real-World Qualitative Results

Figure 16 illustrates the four real-world bimanual manipulation tasks used in our evaluation: *Pour Water*, *Cook Vegetable*, *Tidy Desk*, and *Fold Towel*. These tasks cover precision pouring, insertion, deformable-object manipulation, and long-horizon coordination.

Comparing the execution traces under adversarial perturbation, RePO-VLA responds to forced deviations (e.g., external pushes or object slippage) by synthesizing valid recovery trajectories that resume task progress. In contrast, baseline methods often fail to react to these deviations, leading to task failures.

E1 : Premature Close (Random)



Figure 9: Premature Close (Random)

E2 : Grasp Slip (Clean)

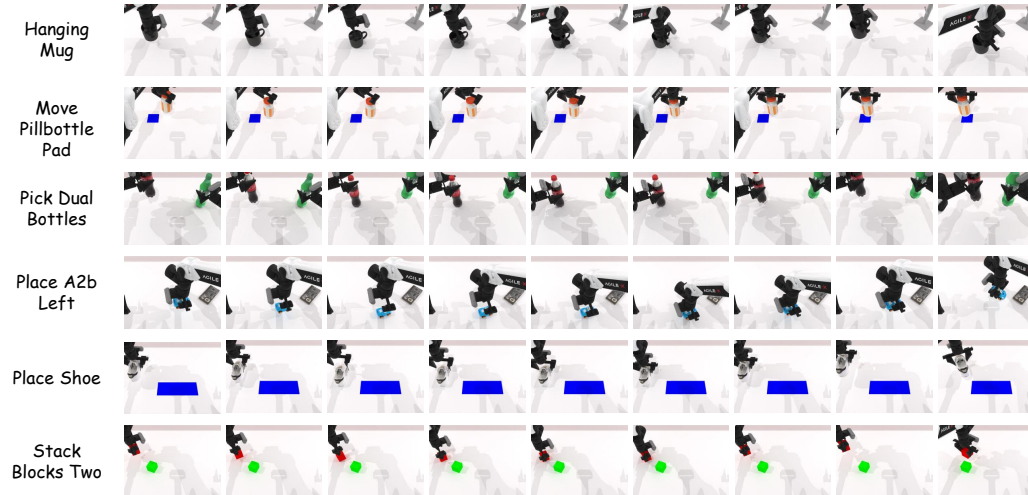


Figure 10: Grasp Slip (Clean)

7 Conclusion

We presented RePO-VLA, a recovery-driven framework for training VLA policies from successful, failed, and recovered trajectories. By combining history-reset recovery initialization with progress-aware value conditioning, RePO-VLA converts mixed-quality interaction data into autonomous corrective behavior. The central result is that failures need not be discarded: their useful pre-failure segments can provide kinematic priors, while their terminal regions can be safely down-weighted through semantic progress labels. Results on FRBench show that explicit recovery supervision and dense value guidance are key ingredients for reliable long-horizon bimanual manipulation.

E2 : Grasp Slip (Random)

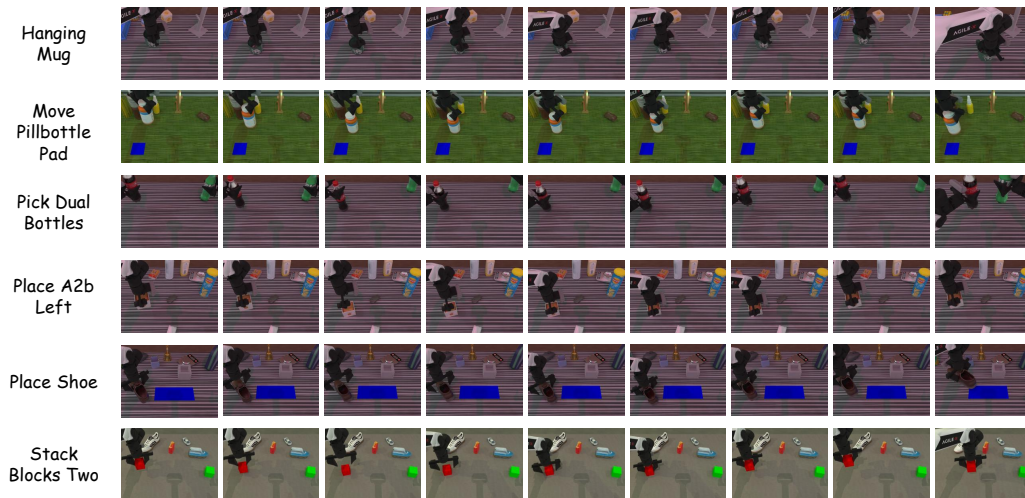


Figure 11: Grasp Slip (Random)

E3 : Grasp Position Offset (Clean)

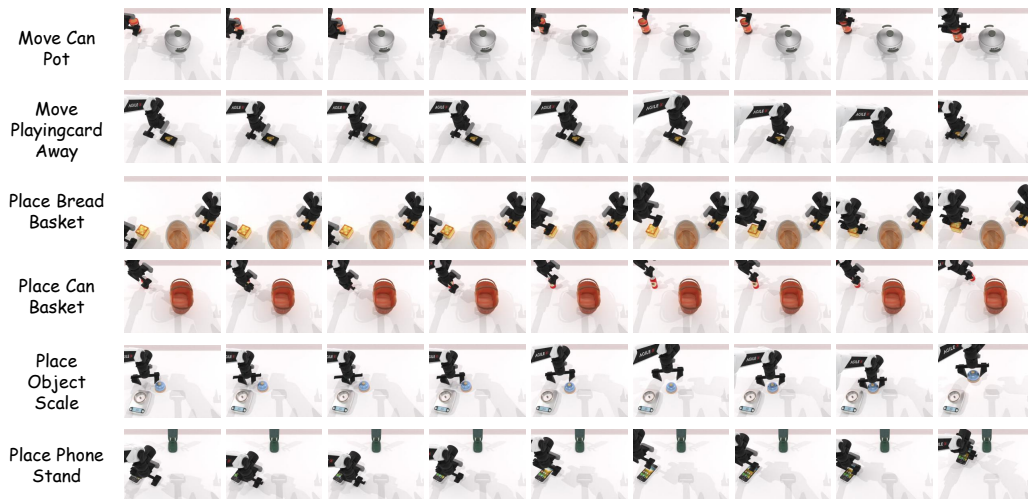


Figure 12: Grasp Position Offset (Clean)

8 Limitations and Future Work

RePO-VLA still relies on observing representative failure modes, so out-of-taxonomy errors can reduce zero-shot recovery. The current iterative data loop can absorb new failures after collection, but broader generalization to unseen physical breakdowns remains open. Real-world Phase II data is also costly because contact dynamics, friction, and deformable interactions are difficult to simulate faithfully, making teleoperated recovery episodes valuable but expensive. Finally, FRBench-Sim does not yet cover fluids or highly deformable objects. Future work will improve sim-to-real recovery data generation, reduce human recovery annotation, and extend FRBench to richer physical media.

E3 : Grasp Position Offset (Random)



Figure 13: Grasp Position Offset (Random)

E4 : Grasp Orientation Mismatch (Clean)

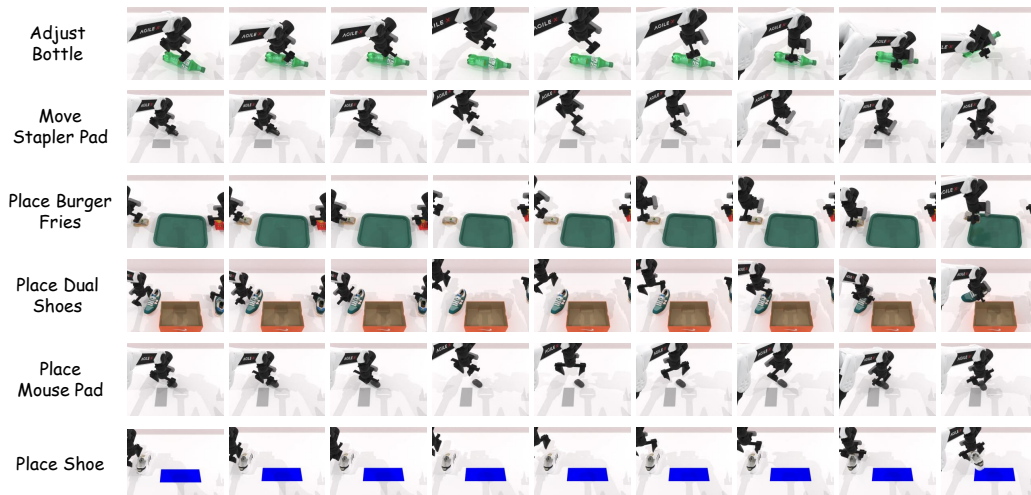


Figure 14: Grasp Orientation Mismatch (Clean)

E4 : Grasp Orientation Mismatch (Random)

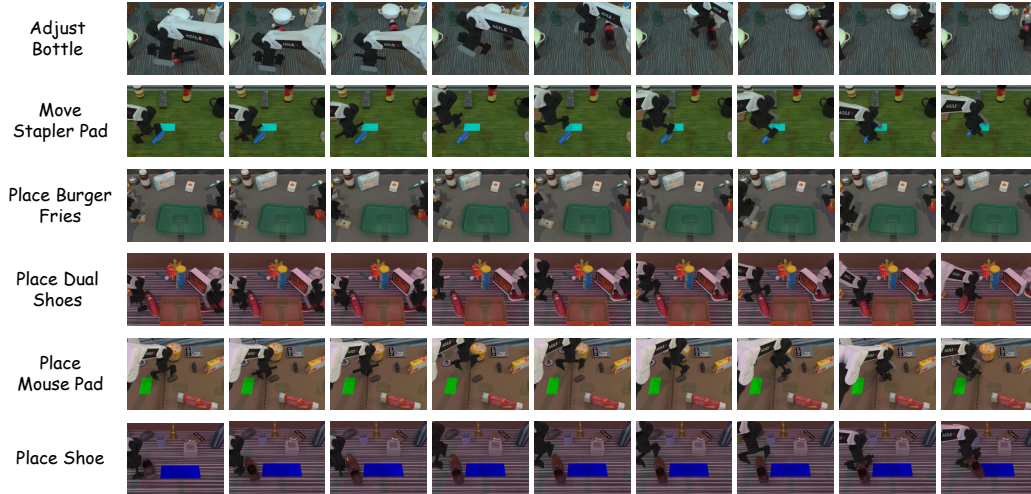


Figure 15: Grasp Orientation Mismatch (Random)



Figure 16: Real-world evaluation tasks. The four contact-rich bimanual settings cover precision pouring, food preparation, desk organization, and deformable-object folding.

References

- Michael Ahn, Anthony Brohan, Noah Brown, Yevgen Chebotar, Omar Cortes, Byron David, Chelsea Finn, Chuyuan Fu, Keerthana Gopalakrishnan, Karol Hausman, et al. Do as i can, not as i say: Grounding language in robotic affordances. *arXiv preprint arXiv:2204.01691*, 2022.
- Mido Assran, Adrien Bardes, David Fan, Quentin Garrido, Russell Howes, Matthew Muckley, Ammar Rizvi, Claire Roberts, Koustuv Sinha, Artem Zholus, et al. V-jepa 2: Self-supervised video models enable understanding, prediction and planning. *arXiv preprint arXiv:2506.09985*, 2025.
- Philip J Ball, Laura Smith, Ilya Kostrikov, and Sergey Levine. Efficient online reinforcement learning with offline data. In Andreas Krause, Emma Brunskill, Kyunghyun Cho, Barbara Engelhardt, Sivan Sabato, and Jonathan Scarlett, editors, *Proceedings of the 40th International Conference on Machine Learning*, volume 202 of *Proceedings of Machine Learning Research*, pages 1577–1594. PMLR, 23–29 Jul 2023.
- Kevin Black, Noah Brown, James Darphinian, Karan Dhabalia, Danny Driess, Adnan Esmail, Michael Robert Equi, Chelsea Finn, Niccolo Fusai, Manuel Y. Galliker, Dibya Ghosh, Lachy Groom, Karol Hausman, Brian Ichter, Szymon Jakubczak, Tim Jones, Liyiming Ke, Devin LeBlanc, Sergey Levine, Adrian Li-Bell, Mohith Mothukuri, Suraj Nair, Karl Pertsch, Allen Z. Ren, Lucy Xiaoyang Shi, Laura Smith, Jost Tobias Springenberg, Kyle Stachowicz, James Tanner, Quan Vuong, Homer Walke, Anna Walling, Haohuan Wang, Lili Yu, and Ury Zhilinsky. $\pi_{0.5}$: a vision-language-action model with open-world generalization. In Joseph Lim, Shuran Song, and Hae-Won Park, editors, *Proceedings of The 9th Conference on Robot Learning*, volume 305 of *Proceedings of Machine Learning Research*, pages 17–40. PMLR, 27–30 Sep 2025a.
- Kevin Black, Noah Brown, Danny Driess, Adnan Esmail, Michael Robert Equi, Chelsea Finn, Niccolo Fusai, Lachy Groom, Karol Hausman, Brian Ichter, Szymon Jakubczak, Tim Jones, Liyiming Ke, Sergey Levine, Adrian Li-Bell, Mohith Mothukuri, Suraj Nair, Karl Pertsch, Lucy Xiaoyang Shi, Laura Smith, James Tanner, Quan Vuong, Anna Walling, Haohuan Wang, and Ury Zhilinsky. π_0 : A vision-language-action flow model for general robot control. In *Proceedings of Robotics: Science and Systems*, Los Angeles, CA, USA, June 2025b.
- Qingwen Bu, Jisong Cai, Li Chen, Xiuqi Cui, Yan Ding, Siyuan Feng, Shenyuan Gao, Xindong He, Xuan Hu, Xu Huang, et al. Agibot world colosseo: A large-scale manipulation platform for scalable and intelligent embodied systems. *arXiv preprint arXiv:2503.06669*, 2025.
- Kang Chen, Zhihao Liu, Tonghe Zhang, Zhen Guo, Si Xu, Hao Lin, Hongzhi Zang, Xiang Li, Quanlu Zhang, Zhaofei Yu, et al. π_{RL} : Online rl fine-tuning for flow-based vision-language-action models. *arXiv preprint arXiv:2510.25889*, 2025a.
- Tianxing Chen, Zanxin Chen, Baijun Chen, Zijian Cai, Yibin Liu, Zixuan Li, Qiwei Liang, Xianliang Lin, Yiheng Ge, Zhenyu Gu, et al. Robotwin 2.0: A scalable data generator and benchmark with strong domain randomization for robust bimanual robotic manipulation. *arXiv preprint arXiv:2506.18088*, 2025b.
- Yuhui Chen, Shuai Tian, Shugao Liu, Yingting Zhou, Haoran Li, and Dongbin Zhao. Conrft: A reinforced fine-tuning method for vla models via consistency policy. In *Proceedings of Robotics: Science and Systems*, Los Angeles, CA, USA, June 2025c.
- Yinpei Dai, Jayjun Lee, Nima Fazeli, and Joyce Chai. Racer: Rich language-guided failure recovery policies for imitation learning. In *2025 IEEE International Conference on Robotics and Automation (ICRA)*, pages 15657–15664. IEEE, 2025.
- Pim de Haan, Dinesh Jayaraman, and Sergey Levine. Causal confusion in imitation learning. In H. Wallach, H. Larochelle, A. Beygelzimer, F. d’Alché-Buc, E. Fox, and R. Garnett, editors, *Advances in Neural Information Processing Systems*, volume 32. Curran Associates, Inc., 2019.
- Yanjiang Guo, Yen-Jen Wang, Lihan Zha, and Jianyu Chen. Doremi: Grounding language model by detecting and recovering from plan-execution misalignment. In *2024 IEEE/RSJ International Conference on Intelligent Robots and Systems (IROS)*, pages 12124–12131. IEEE, 2024.
- Yanjiang Guo, Jianke Zhang, Xiaoyu Chen, Xiang Ji, Yen-Jen Wang, Yucheng Hu, and Jianyu Chen. Improving vision-language-action model with online reinforcement learning. In *2025 IEEE International Conference on Robotics and Automation (ICRA)*, pages 15665–15672. IEEE, 2025.
- Sami Haddadin, Alessandro De Luca, and Alin Albu-Schäffer. Robot collisions: A survey on detection, isolation, and identification. *IEEE Transactions on Robotics*, 33(6):1292–1312, 2017.
- Danijar Hafner, Jurgis Pasukonis, Jimmy Ba, and Timothy Lillicrap. Mastering diverse domains through world models. *arXiv preprint arXiv:2301.04104*, 2023.

- Ryan Hoque, Ashwin Balakrishna, Ellen Novoseller, Albert Wilcox, Daniel S Brown, and Ken Goldberg. Thriftydagger: Budget-aware novelty and risk gating for interactive imitation learning. *arXiv preprint arXiv:2109.08273*, 2021.
- Huang Huang, Fangchen Liu, Letian Fu, Tingfan Wu, Mustafa Mukadam, Jitendra Malik, Ken Goldberg, and Pieter Abbeel. Otter: A vision-language-action model with text-aware visual feature extraction. In Aarti Singh, Maryam Fazel, Daniel Hsu, Simon Lacoste-Julien, Felix Berkenkamp, Tegan Maharaj, Kiri Wagstaff, and Jerry Zhu, editors, *Proceedings of the 42nd International Conference on Machine Learning*, volume 267 of *Proceedings of Machine Learning Research*, pages 25566–25580. PMLR, 13–19 Jul 2025.
- Wenlong Huang, Fei Xia, Ted Xiao, Harris Chan, Jacky Liang, Pete Florence, Andy Zeng, Jonathan Tompson, Igor Mordatch, Yevgen Chebotar, et al. Inner monologue: Embodied reasoning through planning with language models. *arXiv preprint arXiv:2207.05608*, 2022.
- Yunfan Jiang, Chen Wang, Ruohan Zhang, Jiajun Wu, and Li Fei-Fei. Transic: Sim-to-real policy transfer by learning from online correction. In Pulkit Agrawal, Oliver Kroemer, and Wolfram Burgard, editors, *Proceedings of The 8th Conference on Robot Learning*, volume 270 of *Proceedings of Machine Learning Research*, pages 1691–1729. PMLR, 06–09 Nov 2025.
- Moo Jin Kim, Karl Pertsch, Siddharth Karamcheti, Ted Xiao, Ashwin Balakrishna, Suraj Nair, Rafael Rafailov, Ethan P Foster, Pannag R Sanketi, Quan Vuong, Thomas Kollar, Benjamin Burchfiel, Russ Tedrake, Dorsa Sadigh, Sergey Levine, Percy Liang, and Chelsea Finn. Openvla: An open-source vision-language-action model. In Pulkit Agrawal, Oliver Kroemer, and Wolfram Burgard, editors, *Proceedings of The 8th Conference on Robot Learning*, volume 270 of *Proceedings of Machine Learning Research*, pages 2679–2713. PMLR, 06–09 Nov 2025.
- Zijun Lin, Jiafei Duan, Haoquan Fang, Dieter Fox, Ranjay Krishna, Cheston Tan, and Bihan Wen. Failsafe: Reasoning and recovery from failures in vision-language-action models. *arXiv preprint arXiv:2510.01642*, 2025.
- Songming Liu, Lingxuan Wu, Bangguo Li, Hengkai Tan, Huayu Chen, Zhengyi Wang, Ke Xu, Hang Su, and Jun Zhu. Rdt-1b: a diffusion foundation model for bimanual manipulation. In *International Conference on Learning Representations*, 2025.
- Zeyi Liu, Arpit Bahety, and Shuran Song. Reflect: Summarizing robot experiences for failure explanation and correction. *arXiv preprint arXiv:2306.15724*, 2023.
- Ajay Mandlekar, Danfei Xu, Roberto Martín-Martín, Yuke Zhu, Li Fei-Fei, and Silvio Savarese. Human-in-the-loop imitation learning using remote teleoperation. *arXiv preprint arXiv:2012.06733*, 2020.
- Aoran Mei, Guo-Niu Zhu, Huaxiang Zhang, and Zhongxue Gan. Replanvlm: Replanning robotic tasks with visual language models. *IEEE Robotics and Automation Letters*, 9(11):10201–10208, 2024.
- Mitsuhiko Nakamoto, Simon Zhai, Anikait Singh, Max Sobol Mark, Yi Ma, Chelsea Finn, Aviral Kumar, and Sergey Levine. Cal-ql: Calibrated offline rl pre-training for efficient online fine-tuning. *Advances in Neural Information Processing Systems*, 36:62244–62269, 2023.
- Physical Intelligence, Ali Amin, Raichelle Aniceto, Ashwin Balakrishna, Kevin Black, Ken Conley, Grace Connors, James Darpinian, Karan Dhabalia, Jared DiCarlo, et al. $\pi_{0,6}^*$: a vla that learns from experience. *arXiv preprint arXiv:2511.14759*, 2025.
- Pradip Pramanick, Chayan Sarkar, Snehasis Banerjee, and Brojeshwar Bhowmick. Talk-to-resolve: Combining scene understanding and spatial dialogue to resolve granular task ambiguity for a collocated robot. *Robotics and Autonomous Systems*, 155:104183, 2022.
- Shreyas Sundara Raman, Vanya Cohen, Ifrah Idrees, Eric Rosen, Raymond Mooney, Stefanie Tellex, and David Paulius. Cape: Corrective actions from precondition errors using large language models. In *2024 IEEE International Conference on Robotics and Automation (ICRA)*, pages 14070–14077. IEEE, 2024.
- Ralf Römer, Adrian Kobras, Luca Worbis, and Angela P Schoellig. Failure prediction at runtime for generative robot policies. *arXiv preprint arXiv:2510.09459*, 2025.
- Som Sagar, Jiafei Duan, Sreevishakh Vasudevan, Yifan Zhou, Heni Ben Amor, Dieter Fox, and Ransalu Senanayake. Robomd: Uncovering robot vulnerabilities through semantic potential fields. *arXiv preprint arXiv:2412.02818*, 2024.
- Hao Shi, Bin Xie, Yingfei Liu, Lin Sun, Fengrong Liu, Tiancai Wang, Erjin Zhou, Haoqiang Fan, Xiangyu Zhang, and Gao Huang. Memoryvla: Perceptual-cognitive memory in vision-language-action models for robotic manipulation. In *International Conference on Learning Representations*, 2026.

- Lucy Xiaoyang Shi, Zheyuan Hu, Tony Z Zhao, Archit Sharma, Karl Pertsch, Jianlan Luo, Sergey Levine, and Chelsea Finn. Yell at your robot: Improving on-the-fly from language corrections. *arXiv preprint arXiv:2403.12910*, 2024.
- Noah Shinn, Federico Cassano, Ashwin Gopinath, Karthik Narasimhan, and Shunyu Yao. Reflexion: Language agents with verbal reinforcement learning. *Advances in Neural Information Processing Systems*, 36:8634–8652, 2023.
- Marta Skreta, Zihan Zhou, Jia Lin Yuan, Kouros Darvish, Alán Aspuru-Guzik, and Animesh Garg. Replan: Robotic replanning with perception and language models. *arXiv preprint arXiv:2401.04157*, 2024.
- Junjie Wen, Minjie Zhu, Jiaming Liu, Zhiyuan Liu, Yicun Yang, Linfeng Zhang, Shanghang Zhang, Yichen Zhu, and Yi Xu. dvla: Diffusion vision-language-action model with multimodal chain-of-thought. *arXiv preprint arXiv:2509.25681*, 2025a.
- Junjie Wen, Yichen Zhu, Minjie Zhu, Zhibin Tang, Jinming Li, Zhongyi Zhou, Xiaoyu Liu, Chaomin Shen, Yaxin Peng, and Feifei Feng. Diffusionvla: Scaling robot foundation models via unified diffusion and autoregression. In Aarti Singh, Maryam Fazel, Daniel Hsu, Simon Lacoste-Julien, Felix Berkenkamp, Tegan Maharaj, Kiri Wagstaff, and Jerry Zhu, editors, *Proceedings of the 42nd International Conference on Machine Learning*, volume 267 of *Proceedings of Machine Learning Research*, pages 66558–66574. PMLR, 13–19 Jul 2025b.
- Philipp Wu, Yide Shentu, Qiayuan Liao, Ding Jin, Menglong Guo, Koushil Sreenath, Xingyu Lin, and Pieter Abbeel. Robocopilot: Human-in-the-loop interactive imitation learning for robot manipulation. *arXiv preprint arXiv:2503.07771*, 2025.
- Rongtao Xu, Jian Zhang, Minghao Guo, Youpeng Wen, Haoting Yang, Min Lin, Jianzheng Huang, Zhe Li, Kaidong Zhang, Liqiong Wang, Yuxuan Kuang, Meng Cao, Feng Zheng, and Xiaodan Liang. A0: An affordance-aware hierarchical model for general robotic manipulation. In *Proceedings of the IEEE/CVF International Conference on Computer Vision (ICCV)*, pages 13491–13501, October 2025.
- Zwei Ye, Weifeng Lu, Minghao Ye, Tao Lin, Shuo Yang, Junchi Yan, and Bo Zhao. Robofac: A comprehensive framework for robotic failure analysis and correction. *arXiv preprint arXiv:2505.12224*, 2025.
- Hongyin Zhang, Zifeng Zhuang, Han Zhao, Pengxiang Ding, Hongchao Lu, and Donglin Wang. Reinbot: Amplifying robot visual-language manipulation with reinforcement learning. In Aarti Singh, Maryam Fazel, Daniel Hsu, Simon Lacoste-Julien, Felix Berkenkamp, Tegan Maharaj, Kiri Wagstaff, and Jerry Zhu, editors, *Proceedings of the 42nd International Conference on Machine Learning*, volume 267 of *Proceedings of Machine Learning Research*, pages 77254–77271. PMLR, 13–19 Jul 2025.
- Kaidong Zhang, Jian Zhang, Rongtao Xu, Yu Sun, Shuoshuo Xue, Youpeng Wen, Xiaoyu Guo, Minghao Guo, Weijia Liufu, Zihou Liu, Kangyi Ji, Yangsong Zhang, Jiarun Zhu, Jingzhi Liu, Zihang Li, Ruiyi Chen, Meng Cao, Jingming Zhang, Shen Zhao, Xiaojun Chang, Feng Zheng, Ivan Laptev, and Xiaodan Liang. A1: A fully transparent open-source, adaptive and efficient truncated vision-language-action model. *arXiv preprint arXiv:2604.05672*, 2026.
- Zijian Zhang, Kaiyuan Zheng, Zhaorun Chen, Joel Jang, Yi Li, Siwei Han, Chaoqi Wang, Mingyu Ding, Dieter Fox, and Huaxiu Yao. Grape: Generalizing robot policy via preference alignment. *arXiv preprint arXiv:2411.19309*, 2024.
- Fangqi Zhu, Zhengyang Yan, Zicong Hong, Quanxin Shou, Xiao Ma, and Song Guo. Wmpo: World model-based policy optimization for vision-language-action models. In *International Conference on Learning Representations*, 2026.